

Modified Method of Characteristics for Simulating Microscale Energy Transport

Laurent Pilon*

e-mail: pilon@seas.ucla.edu

Kamal M. Katika

Mechanical and Aerospace Engineering
Department, Henri Samuelli School of
Engineering and Applied Science,
University of California, Los Angeles
Los Angeles, CA 90095

This paper presents a new numerical scheme for simulating multidimensional transient and steady-state microscale energy transport. The new method is based on the method of characteristics that follows heat carriers along their pathline. Unlike traditional methods, it uses a fixed computational grid and follows the heat carriers backward in time. The method 1) is accurate, 2) is unconditionally stable, 3) can deal with complex geometries without a large increase in computational cost, and 4) can be used for solving coupled equations using other numerical schemes. First, the numerical scheme is described. Then, simulations for transient and steady-state phonon transport in dielectric thin films are discussed. Numerical results are compared with analytical and reported numerical solutions and good agreement is obtained. [DOI: 10.1115/1.1795233]

Keywords: Heat Conduction, Microscale, Nanoscale, Heat Transfer, Boltzmann Transport Equation

1 Introduction

During the last decade, heat transfer at microscale has been the object of intense studies [1,2]. The research effort has been driven by important applications in microelectronics, thin films, nanomaterials, and short-pulse laser heating. The conventional approach to heat conduction problems using macroscopic empirical laws such as Fourier's law or Joule's law of heat generation break down when the length scale of the system is comparable to the energy carrier mean free path or when the time scale of the physical process is smaller than the relaxation time of the heat carriers [2,3]. Then, transport of heat carriers must be treated in greater details.

Heat is transported by carriers comprising of electrons, phonons, and photons. Heat conduction is dominated by phonons in dielectric materials, predominantly by electrons in pure metals, and by both phonons and electrons in impure metals or alloys [4]. In all cases, transport of the heat carriers is governed by the Boltzmann transport equation (BTE). The density function of heat carriers can be described in a state space consisting not only of the physical space but also of an abstract wavevector space. In the physical space, the state vector coordinates consist of the spatial coordinates [e.g., (x, y, z) in Cartesian coordinates]. In the wavevector space, the system is characterized by its wavevector \vec{k} . Considering electron and phonon transport, the state vector \vec{S} can be expressed as $\vec{S} = [\vec{r}, \vec{k}, t]$. Let f_p be the distribution function of the energy carriers in the polarization state p . The distribution function $f_p(\vec{r}, \vec{k}, t)$ is assumed to be sufficiently smooth to allow differentiation with respect to any of its variables as many times as necessary [5]. Then, the BTE can be expressed as [6]

$$\frac{\partial f_p}{\partial t} + \vec{v} \cdot \nabla_x f_p + \frac{d\vec{k}}{dt} \cdot \nabla_k f_p = \left(\frac{\partial f_p}{\partial t} \right)_{sca} \quad (1)$$

where \vec{v} and \vec{k} are the group velocity vector (velocity of energy propagation) and wavevector of the heat carriers, respectively. The operators ∇_x and ∇_k are the gradient operators in the physical and wavevector space, respectively. The second term on the left-hand side of Eq. (1) represents the advection of the distribution,

while the third term corresponds to the change of momentum caused by external fields relating to the particle acceleration. Finally, the term $(\partial f_p / \partial t)_{sca}$ on the right-hand side of Eq. (1) represents the restoration of thermodynamic equilibrium due to scattering by electrons, holes, defects in the lattice, and phonons [7].

Different formulations of the BTE have been developed in recent years to solve engineering problems. The first alternative formulation to the BTE for phonon transport has been developed by Majumdar [3], who recognized that the flux of energy per unit time, per unit area, per unit solid angle in the direction \vec{s} , and per unit frequency interval around ω can be written as

$$I_\omega(\vec{r}, \vec{s}, \omega, t) = \frac{1}{4\pi} \sum_{p=1}^3 \hbar \omega v_p f_p(\vec{r}, \vec{s}, \omega, t) \mathcal{D}_p(\omega) \quad (2)$$

where \vec{s} is the unit vector in the direction of carrier propagation, $\hbar \omega$ is the heat carrier energy, while v_p and $\mathcal{D}_p(\omega)$ are the speed of sound and the phonon density of states per unit volume for each polarization, respectively. The summation is over the three phonon polarization states [3,4]. The resulting form of the BTE has been named the equation of phonon radiative transfer (EPRT) [3].

Another common approach used for electron transport consists of solving for one or several moments of the distribution function [6,7]. A partial differential equation for each moment can be derived from the BTE to assure conservation of charge, momentum, and energy resulting in the so-called hydrodynamic equations. They are the governing equations for the electron density n_e , momentum \vec{p}_e , and energy E_e and can be derived by integrating the BTE over all frequencies and after multiplying it by 1, $p_e = m_e^* \vec{v}_e$, and $E_e = p_e^2 / 2m_e^*$, respectively. Hydrodynamic equations are often solved instead of the BTE. The moment method has the advantage of reducing computational times, a valuable feature in control and optimization [5]. However, the discrete formulation has major drawbacks that have been discussed extensively by Kumar and Ramkrishna [8,9]. In brief, the discrete formulation lacks of *internal consistency*, i.e., some of the moments of the particle density function f_p (or of the spectral intensity) cannot be predicted accurately. The calculation is designed for certain arbitrarily selected moments of the particle density function rather than for an estimate of the particle density function accurate enough for estimating *all* moments of the population [5]. For example, an important moment includes the energy flux due to electrons \vec{q}_e expressed as,

*Corresponding author.

Contributed by the Heat Transfer Division for publication in the JOURNAL OF HEAT TRANSFER. Manuscript received by the Heat Transfer Division June 11, 2003; revision received February 20, 2004. Associate Editor: C. P. Grigoropoulos.

$$\vec{q}_e(\vec{r}, t) = \int \epsilon \vec{v}_e f_e(\vec{r}, \epsilon, t) \mathcal{D}(\epsilon) d\epsilon \quad (3)$$

More recently, Chen [10] derived the ballistic-diffusion heat conduction equations by dividing the phonon distribution function into the carriers originating from the boundaries and the carriers originating from the medium. Governing equations and boundary conditions for each component (ballistic or diffuse) of the distribution have been derived from the BTE.

Even though the formulation of the thermal transport at microscale has long been established [4], experiments of heat transfer at subcontinuum scale poses great challenges, and numerical simulations have become critical to the fundamental understanding of the phenomena and to the engineering design of submicron electronic devices [11]. As recognized by different authors [1,3], the major difficulty lies in solving the BTE or the subsequent equations.

Due to the analogy between the radiative transfer equation (RTE) and the Boltzmann transport equation [3], the traditional numerical methods employed for solving the radiative transfer equation have been used to solve the EPRT [3,11–13]. For example, Joshi and Majumdar [12] used the Schuster-Schwarzschild two-flux approximation to solve the transient and steady-state heat conduction across a diamond thin film. In the case of steady-state heat conduction along a dielectric thin film with specular phonon reflection at the boundary, Klitsner et al. [14] solved the BTE using the Monte Carlo simulations while Majumdar [3] solved the EPRT using the discrete ordinate method of Kumar et al. [15]. In both cases, the dielectric thin film was assumed to be a gray medium. Traditional discrete ordinate methods have also been used by other researchers [13]. More recently, Murthy and Mathur [11] proposed the use of unstructured solution-adaptive finite volume methods. Each one of these methods has some advantages and drawbacks.

Finite difference or finite volume methods are widely used in engineering to solve partial differential equations. Numerical solutions of relatively simple problems are readily and efficiently found by using these techniques, particularly for steady states. However, major drawbacks include 1) false scattering due to inadequate spatial discretization of the transient BTE, which leads to smearing of the wavefront [16], 2) the numerical instability that may force one to reduce the time step or the finite volume dimensions, 3) the formulation and the computing requirements increase greatly for problems of complex geometry and anisotropic behavior of the medium [17], and 4) the ray effect due to angular discretization can cause “large errors in the prediction of the equivalent temperature unless fine angular discretizations are used, particularly at low acoustic thicknesses,” as recognized by Murthy and Mathur [18]. The authors combined a ray-tracing technique with the finite volume method to improve predictions of the method [18].

The discrete ordinate method (DOM) is another popular method for solving the RTE or the BTE for neutrons and phonons [3,17]. The equation is solved for an arbitrary set of discrete directions. The integrations over the solid angle are approximated by numerical quadrature. In multidimensional problems, spatial partial derivatives can be computed using finite volume methods. Then, the DOM has the same advantages and drawbacks as finite volume methods. Specific drawbacks of the DOM include 1) the “ray effect” that may be significant at low optical thickness and for transient simulations, as discussed in details by Murthy and Mathur [18], 2) the difficulty to deal with specularly reflecting boundaries since the reflected or transmitted beams might not coincide with the discrete ordinates, 3) the arbitrary choice of the quadrature that may result in significantly different numerical results [19], 4) the method does not assure conservation of radiative energy [20], and 5) false scattering.

Finally, solving transport equations by the Monte Carlo technique consists of tracing the history of a statistically meaningful random sample of particles from their point of birth to their point

of death. The advantages of the Monte Carlo method are its ability to handle complex problems in terms of geometry and spatial and directional dependency without significantly increasing the computing effort or the complexity of the formulation [17]. Major drawbacks include: 1) the higher computational cost than traditional methods for relatively simple problems, 2) the difficulty to couple the method to other methods such as finite difference, 3) the statistical error intrinsic to any statistical methods, and 4) the inefficiency to deal with problems considering the radiative intensity onto a small surface and/or a small range of solid angles. Modest [21] addressed the last issue by using backward Monte Carlo simulations.

The present study aims at presenting a new numerical scheme for solving thermal transport at submicron scales. We recognize that the BTE and subsequent equations fall in the framework of population balance theory, whose mathematical formalism has been recently reviewed by Ramkrishna [5]. The modified method of characteristics developed by Pilon and Viskanta [22] for solving multiphase particulate flows has been adapted to solve multidimensional transient and steady-state microscale heat conduction problems. First, the numerical method is described. Then, test problems are solved and the numerical solutions obtained are compared with analytical or numerical solutions already reported.

2 Governing Equations

The BTE applies to both electron and phonon transport. However, the present study is limited to phonon transport in dielectric materials. In order to compare the present numerical method with existing ones, the study focuses on the EPRT [3]. This section reviews the assumptions traditionally made to make the problem mathematically tractable. Then, the governing equation and the associated boundary conditions are derived.

2.1 Assumptions. The following assumptions are usually made for solving the EPRT for phonon transport at microscale in engineering applications dealing with dielectric materials such as diamond and silicon dioxide [3,6,7,10]:

1. Phonons are considered to be the only heat carriers.
2. Phonon transport is assumed to satisfy the Boltzmann transport equation. Regimes of heat conduction and conditions for validity of the BTE have been discussed by Tien and Chen [1].
3. The Debye model is assumed to be valid, thus [4]

- The phonon group velocity \vec{v}_p is considered to be constant (independent of frequency and time) with $\vec{v}_p = v_p \vec{s}$, where v_p is the speed of sound in the materials for polarization p in direction \vec{s} . The dispersion relation is given by $\omega_p = v_p k$ and the group velocity, being constant, leads to $dk/dt = 0$. Physically, phonons dominating the heat transport travel at the speed of sound which does not vary significantly over the dominating range of frequency for heat transfer [3].
- The phonon modes of frequency cannot be larger than the Debye frequency ω_D defined as [4],

$$\omega_D = \frac{k_B \theta_D}{\hbar} \quad (4)$$

where θ_D is the Debye temperature. Physically, it corresponds to the fact that phonons cannot assume wavelengths smaller than twice the atomic spacing [7].

- The number of energy levels per unit of energy range for each polarization, the so-called density of states, is assumed to be continuous, denoted $\mathcal{D}_p(\omega)$, and given by [4]

$$\mathcal{D}_p(\omega) = \frac{\omega^2}{2\pi^2 v_p^3} \quad \text{with} \quad 0 \leq \omega \leq \omega_D \quad (5)$$

4. The polarization effects are negligible and all polarizations are treated identically.

5. The single mode relaxation time approximation is used to express the scattering term of the BTE, i.e., [3,4],

$$\left(\frac{\partial I_\omega}{\partial t}\right)_{sca} = \frac{I_\omega^0 - I_\omega}{\tau_s(\omega)} = \frac{\frac{1}{2} \int_{-1}^1 I_\omega d\mu - I_\omega}{\tau_s(\omega)} \quad (6)$$

where θ is the polar angle, μ is the director cosine, i.e., $\mu = \cos \theta$, and I_ω^0 is the equilibrium phonon blackbody radiation intensity. The phonon scattering rate $1/\tau_s$ is assumed to be the sum of the scattering rates associated to 1) scattering on lattice imperfections $1/\tau_i$ and 2) three phonon inelastic Umklapp scattering $1/\tau_U$. Even though the normal (N) three phonon inelastic scattering processes indirectly influence energy transfer, they are neglected here for the sake of simplicity, and to permit comparison with previous studies [3,11] and validation of the method. Note that this assumption does not reduce the generality of the method since N processes can also be accounted for by using the relaxation time approximation [3].

6. The medium and the scattering processes are assumed to be isotropic, thus the relaxation time depends only on frequency $[\tau_s(\vec{r}, \vec{k}) = \tau_s(\omega)]$ [10].
 7. The contribution of the optical phonons to heat transfer is neglected due to their small velocity [7].
 8. The phase of the lattice waves is not considered, thus neglecting interferences.
 9. Thermal expansion is neglected [4].

Following the above assumptions, the equation of phonons radiative transfer (EPRT) can be derived from Eqs. (1), (2), and (6) as [3]

$$\frac{\partial I_\omega}{\partial t} + \vec{v} \cdot \nabla_x I_\omega = \frac{\frac{1}{2} \int_{-1}^1 I_\omega d\mu - I_\omega}{\tau_s(\omega)} \quad (7)$$

At temperatures much lower than the Debye temperature, the recovery of the temperature from the intensity $I_\omega(\vec{r}, \omega, t)$ can be performed by defining an equivalent equilibrium temperature from the following equation [3,11]:

$$\begin{aligned} \frac{\sigma [T(\vec{r}, t)]^4}{\pi} &= \frac{1}{4\pi} \int_0^{\omega_D} \int_0^{2\pi} \int_0^\pi I_\omega(\vec{r}, t) \sin \theta d\theta d\phi d\omega \\ &= \frac{1}{2} \int_0^{\omega_D} \int_{-1}^1 I_\omega(\vec{r}, t) d\mu d\omega \end{aligned} \quad (8)$$

where σ is the Stefan-Boltzman constant for phonons, given by

$$\sigma = \frac{\pi^2}{40} \frac{k_B^4}{\hbar^3 \nu} \quad (9)$$

Note that Eq. (8) can be used, at any temperature, for gray medium calculations which neglect the spectral dependence of the intensity [11].

2.2 Boundary Conditions. We limit our study to thermalizing boundaries and specularly reflecting boundaries.

Thermalizing Boundaries. At a thermalizing boundary, the temperature is prescribed. The interface absorbs all incident phonons [23] and emits blackbody phonon radiation assumed to be at equilibrium at the prescribed temperature T . Thus, the boundary conditions at the thermalizing boundaries yields the isotropic spectral radiation intensity according to

$$I_{b,\omega} = \frac{3\hbar^3 \omega^3}{8\pi^3 \nu^2 [e^{\hbar\omega/k_B T} - 1]} \quad (10)$$

For a gray medium, the thermalizing boundary condition for the total intensity becomes

$$I_b = \sigma T^4 / \pi \quad (11)$$

Specularly Reflecting Boundaries. A specularly reflecting boundary with an outward normal vector \vec{n} corresponds to an adiabatic interface at which [11]

$$I_\omega(\vec{r}_b, \vec{s}, t) = I_\omega(\vec{r}_b, \vec{s}_r, t) \quad (12)$$

with $\vec{s}_r = \vec{s} - 2(\vec{s} \cdot \vec{n})\vec{n}$ and \vec{r}_b is the spatial coordinates of the boundary. Specularly reflecting boundaries represent an ideal behavior achieved by acoustically smooth surfaces, i.e., the surface roughness is much smaller than the phonon wavelength.

3 Modified Method of Characteristics

The method of characteristics consists of transforming the partial differential BTE into an ordinary differential equation solved along the pathline of the heat carriers. The conventional implementation (or *direct marching method*) of the method of characteristics is based on the Lagrangian formulation: the heat carriers are identified and located at initial time $t=t_0$ and followed at subsequent time as they are transported. In 3D thermal transport, however, the deformation that the initial mesh undergoes as time progresses leads to deterioration of the numerical solution [24].

The modified method of characteristics (or *inverse marching method*) is an interpretation of the Lagrangian approach that overcomes the difficulties related to mesh deformation [24]. Unlike the direct marching method, the inverse marching method uses a fixed grid of arbitrary shape. In the remaining of the present study, we consider a Cartesian coordinate system for illustration purposes. However, the approach can be generalized to any system of coordinates. By definition, the total time derivative of $I_\omega = I_\omega(x, y, z, t)$ with respect to time t in the direction (θ, ϕ) can be written as

$$\frac{dI_\omega}{dt} = \frac{\partial I_\omega}{\partial t} + \frac{dx}{dt} \frac{\partial I_\omega}{\partial x} + \frac{dy}{dt} \frac{\partial I_\omega}{\partial y} + \frac{dz}{dt} \frac{\partial I_\omega}{\partial z} \quad (13)$$

We further define the characteristic curves in the physical space as

$$\frac{dx}{dt} = \nu \sin \theta \cos \phi \quad (14)$$

$$\frac{dy}{dt} = \nu \sin \theta \sin \phi \quad (15)$$

$$\frac{dz}{dt} = \nu \cos \theta \quad (16)$$

Then, along the characteristic curves in the (x, y, z, t) space, the BTE can be written as

$$\frac{DI_\omega}{Dt} = \frac{\frac{1}{2} \int_{-1}^1 I_\omega d\mu - I_\omega}{\tau_s(\omega)} \quad (17)$$

where DI_ω/Dt denotes the substantial derivative of I_ω , i.e., the total time derivative along the pathline of the energy carriers.

Figure 1 shows a 3D computational cell in Cartesian coordinates. The modified method of characteristics consists of determining the coordinates (x_n, y_n, z_n) of the point in space from where the particles located at the grid point (x_a, y_b, z_c) at time $t + \Delta t$ originated from at time t while traveling in the direction of polar angle θ_n and azimuthal angle ϕ_l . In other words, for each point of a specified grid, the pathline is projected rearward along the characteristic curve to the initial data surface to determine the initial data point. For example, in Fig. 1 the point (x_a, y_b, z_c) is the point $(x_{i+1}, y_{j+1}, z_{k+1})$. The solid line represents the section of the characteristic curve along which the particle traveled from location (x_n, y_n, z_n) to location (x_a, y_b, z_c) during the time interval between t and $t + \Delta t$.

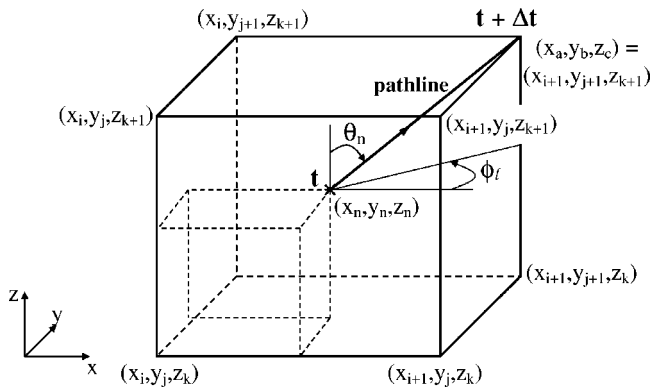


Fig. 1 Typical computational cell used for inverse marching method containing the pathline of the phonons

The general block diagram of the numerical procedure for solving the EPRT using the modified method of characteristics is shown in Fig. 2. First, temperature and spectral radiation intensity are set to their initial values across the computational domain. To avoid numerical instabilities, it is necessary to insure that the phonons do not leave the computational cell between the time t and $t + \Delta t$. In other words, each computational cell traveled by the phonons should contain at least one point on the characteristic

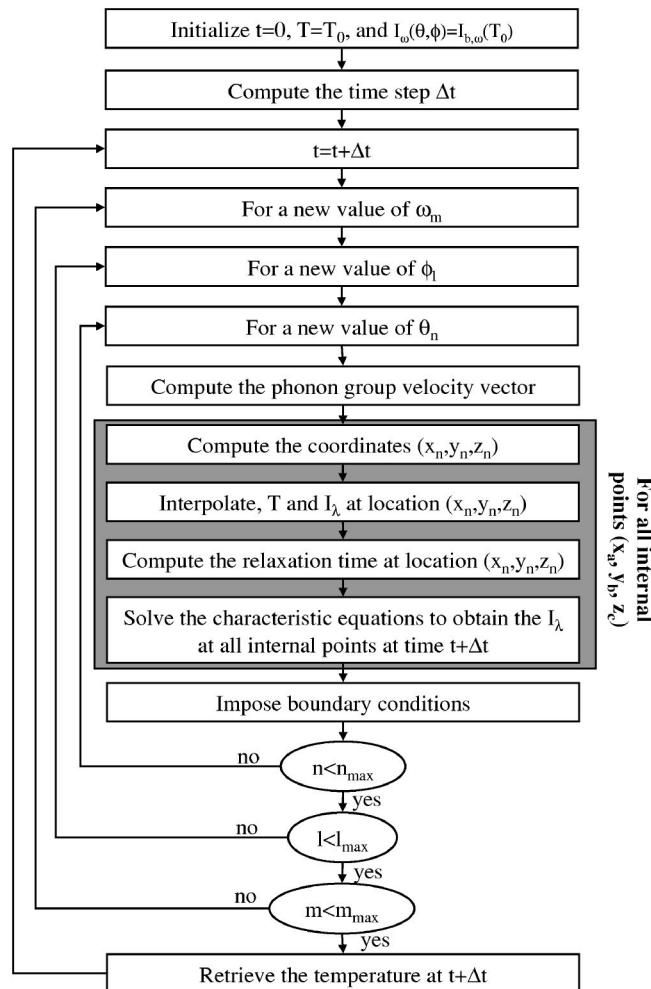


Fig. 2 Block diagram of the numerical procedure for solving the spectral EPRT by the modified method of characteristics

curve, i.e., the point (x_n, y_n, z_n) is always in a computational cell adjacent to (x_a, y_b, z_c) . Therefore, the time step Δt for the entire calculation is determined by the equation,

$$\Delta t = \min \left\{ \left| \frac{x_{i+1} - x_i}{v} \right|, \left| \frac{y_{j+1} - y_j}{v} \right|, \left| \frac{z_{k+1} - z_k}{v} \right| \right\} \quad (18)$$

For a given frequency ω_m , a polar angle θ_n , an azimuthal angle ϕ_l , and for all internal grid points (x_a, y_b, z_c) where phonons are located at time $t + \Delta t$, the phonon's position (x_n, y_n, z_n) at time t is calculated as

$$x_n = x_a - v \sin \theta_n \cos \phi_l \Delta t \quad (19)$$

$$y_n = y_b - v \sin \theta_n \sin \phi_l \Delta t \quad (20)$$

$$z_n = z_c - v \cos \theta_n \Delta t \quad (21)$$

The values of the variables T and I_ω at point (x_n, y_n, z_n) and time t are obtained by Lagrangian interpolation using their values at time t at the eight corners of the computational cell in which (x_n, y_n, z_n) is located. Then, the ordinary differential Eq. (17) is solved forward in time by the fourth-order Runge-Kutta method at location (x_a, y_b, z_c) and time $t + \Delta t$ at all interior points and out-flow boundaries. The integrals appearing in Eqs. (8) and (17) are estimated by the 3/8 Simpson numerical integration method [25]. Finally, the boundary conditions are imposed in directions pointing toward the medium. The calculations are repeated for all the discretized values of frequency ω_m , polar angle θ_n , and azimuthal angle ϕ_l . The temperature at all grid points is recovered from Eq. (8) before the temperature and intensity fields are computed at the next time step.

The advantages and drawbacks of the modified method of characteristics over other methods are the following:

- Unlike finite-difference methods, in which the information propagates along coordinate lines, the method of characteristics propagates the information along the heat carriers' pathlines and thus matches the physics of the energy transport, resulting in extremely accurate numerical results.
- It does not require any outflow boundary conditions [26]. For this reason, the modified method of characteristics is recommended for hyperbolic equations such as the BTE, whose solution has a distinct domain of dependence and range of influence [25].
- The method can be used for solving coupled equations such as the BTE for electrons, the radiative transfer equation for photons, and/or the Maxwell's equations. Other numerical schemes such as finite-difference or finite element methods can also be used in combination with the present method.
- It can be used for both transient and steady-state calculations with great accuracy and without problems of numerical instability.
- Unlike finite-volume methods, there is no practical restriction on the aspect ratio of computational cells [27]. Here, on the contrary, the cell size is solely determined based on accuracy requirements, and any arbitrary set of points can be used as the computational grid.
- It may be more time consuming than other methods due to interpolations and numerical integrations. However, the computational time does not increase significantly as the geometry becomes more involved, or coupling with other heat carriers or fluid flow takes place.

4 Results and Discussion

For validation purposes, the results obtained by the modified method of characteristics for a set of test problems have been compared with analytical solutions or results reported in the literature using different numerical schemes. The cases considered are 1) transient and steady-state ballistic transport, 2) transient and

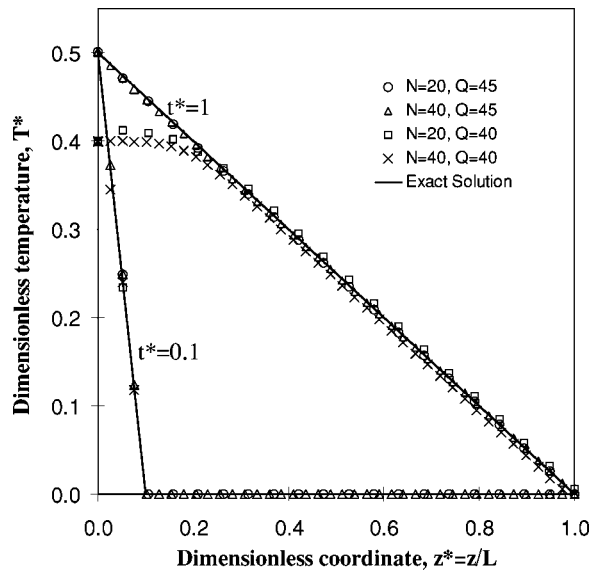


Fig. 3 Numerical solution for transient heat conduction in the ballistic limit for a 1 μm thick gray diamond type IIa thin film with black bounding surfaces using different grids and 30 directions

steady-state heat conduction across a diamond film, and 3) 2D steady-state heat conduction along a gray thin film with specularly reflecting boundaries.

4.1 Ballistic Transport. In order to validate the numerical method described previously, transient and steady-state heat conduction in dielectric thin films in the ballistic transport limit is considered, i.e., phonon scattering is neglected. We further assume that the spectral phonon intensity I_ω is independent of wavelength (gray behavior). Under these assumptions, the EPRT simplifies to [11]

$$\frac{\partial I}{\partial t} + \vec{v} \cdot \nabla I = 0 \quad (22)$$

where I is the total phonon intensity.

Transient Calculations. Two-dimensional numerical simulations were performed for a $10 \mu\text{m} \times 1 \mu\text{m}$ diamond type IIa polyhedral thin film initially at 300 K. At $t=0$, the bottom temperature $T(x, y, 0) = T_1$ is imposed to be 301 K while the top temperature T_2 is maintained at 300 K. The boundary conditions at the thermalizing boundaries in directions pointing toward the medium were $I(x, y, 0, t) = \sigma T_1^4 / \pi$ and $I(x, y, L, t) = \sigma T_2^4 / \pi$, respectively, while symmetry boundary conditions were imposed at the other surfaces. The width of the thin film is considered much larger than its thickness so that heat conduction can be treated as 1D. The temperature at each node was retrieved from the computed value of the total radiation intensity I based on the expression

$$T(x, y, z, t) = \left[\frac{\pi}{2\sigma} \int_{-1}^1 I(x, y, z, \mu, t) d\mu \right]^{1/4} \quad (23)$$

Furthermore, in order to simplify the presentation of the results, normalized temperature T^* , time t^* , and location z^* are defined, respectively, as

$$T^*(z^*) = \frac{T^4(z^*) - T_2^4}{T_1^4 - T_2^4}, \quad t^* = \frac{t}{L/\nu}, \quad \text{and} \quad z^* = z/L \quad (24)$$

The computational domain was discretized in a $10 \times N$ grid and Q discrete ordinate directions μ_i per quadrant with N and Q varying from 20 to 40 and from 8 to 50, respectively. Figure 3 shows the

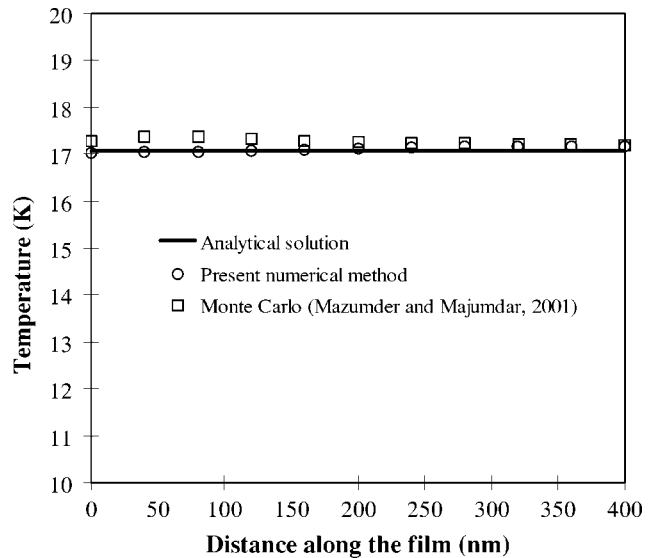


Fig. 4 Numerical solution for steady-state heat conduction in the ballistic limit for a 400 nm thick gray gallium arsenide thin film with black bounding surfaces

numerical results for the normalized temperature T^* as a function of the dimensionless location z^* for dimensionless times $t^* = 0.1$ and 1 for different spatial discretizations. The number of discretizations in the z direction does not affect the ability of the code to capture the propagating front while the number of directions influences the accuracy on the retrieved temperature. Furthermore, the number of grid points in the x and y directions had no effect, due to the symmetry of the problem, and 10 grid points were arbitrarily chosen. Good agreement with theoretical values is observed at both times for 20 cells in the z direction or finer grids and more than 45 directions per quadrant with time step $\Delta t = L/20\nu$. The large number of directions is due to the fact that the integral term is computed by numerical integration. As time increases, the temperature gradient across the film decreases and coarser grids can be used to capture the spatial change of temperature across the film. This must be compared with recent simulations by Murthy and Mathur [11,18] who reported 100 cells, $\Delta t = L/1000\nu$, and 8 discrete directions per quadrant. The authors used an unstructured finite volume scheme to solve the same test problem and recognized that “the problem is quite challenging from a numerical solution point of view,” and that “good spatial and temporal accuracy is required to minimize the numerical diffusion that tends to smear the step solution.” On the contrary, this study shows the advantages of the modified method of characteristics in that the method is unconditionally stable and both transient profile and wavefront are perfectly captured without any smeared front even with coarse grids.

Steady-State Calculations. Steady-state heat conduction across a 400 nm thick gallium arsenide film with black bounding surfaces in the ballistic limit is now considered. One face of the film is maintained at temperature $T(x, y, 0) = T_1 = 10$ K while the other face is maintained at $T(x, y, L) = T_2 = 20$ K. The exact solution to this problem is known to be uniform across the film and equal to $T(z) = [(T_1^4 + T_2^4)/2]^{1/4} = 17.075$ K with a discontinuity at the boundaries. The numerical results were obtained with a 10×11 grid and 45 directions per quadrant for a CPU time of less than 40 seconds on a 633 MHz Pentium III microprocessor. Figure 4 compares the numerical results with the analytical solution and those reported in the literature [28]. The maximum error between the two solutions is less than 0.6% compared to 2% obtained by Mazumder and Majumdar [28] using the Monte Carlo method. Note that an even better precision can be obtained by simulating a

Table 1 Physical properties of type IIa diamond 0.07% of ^{13}C isotope at room temperature [3]

Property	Value
Stefan-Boltzmann constant, σ	50.47 W/m ² K ⁴
Speed of sound, ν	12,288 m/s
Impurity density, η	$0.154 \times 10^{26}/\text{m}^3$
Radius of lattice imperfections, R	1.785 Å
Constant, A	163.94
Umklapp scattering constant, γ	1.58
Debye Temperature, θ_D	1860 K

longer time or by increasing the number of directions. On the contrary, the Monte Carlo method contains intrinsic statistical errors. Finally, the heat flux was computed and found to be constant and independent of location.

4.2 One-Dimensional Heat Conduction Across a Diamond Film. We now consider 1D heat conduction across a diamond type IIa thin film with 0.07% impurity concentration of ^{13}C . The film, of thickness L , is initially at $T=T_0$. At $t=0$, a temperature difference $\Delta T=1$ K is imposed across the film, while the cooler surface is maintained at temperature T_0 . Moreover, only scattering by lattice imperfections and Umklapp scattering are considered [3]. The relaxation time for imperfection scattering τ_i is expressed as [3]

$$\tau_i = \frac{1}{\alpha \varphi \eta \nu} \quad (25)$$

where α is a constant close to unity, η is the number of scatterings site per unit volume, and φ is the scattering cross section expressed as

$$\varphi = \pi R^2 \left(\frac{\chi^4}{\chi^4 + 1} \right) \quad \text{with} \quad \chi = \frac{\omega R}{\nu} \quad (26)$$

with R being the radius of the lattice imperfections. On the other hand, the relaxation time due to Umklapp scattering τ_U is expressed as [3]

$$\tau_U = A \frac{T}{\omega \theta_D} \exp\left(\frac{\theta_D}{\gamma T}\right) \quad (27)$$

where A and γ depend on the materials, while θ_D is the Debye temperature defined as $\theta_D = \hbar \omega_D / k_B$. The overall relaxation time is defined as $1/\tau_s = 1/\tau_i + 1/\tau_U$. Constants and properties required to compute the relaxation times for diamond type IIa with 0.07% impurity concentration of ^{13}C were taken from the literature [3] and are summarized in Table 1. A similar problem has been solved by Majumdar [3] using the discrete ordinate method proposed by Kumar et al. [15] with 8 discrete directions per quadrant. Moreover, the Stefan-Boltzmann constant for phonons is constant and Eq. (8) is valid only for low temperatures (less than 150 K for diamond type IIa). Therefore, in the present study the initial temperature T_0 has been arbitrarily set to 100 K.

Following Majumdar's work [3] and in order to cover the acoustically thin and thick regimes, three different film thicknesses ($L=0.1 \mu\text{m}$, $1 \mu\text{m}$, and $10 \mu\text{m}$) have been considered for type IIa diamond. The calculations were performed on a spectral basis over the frequency range from 0 to ω_D . A converged solution was obtained for a 5×21 grid and 30 directions per quadrant, while the spectrum from 0 to ω_D was discretized into 90 different wavelengths. Figure 5 shows the transient evolution of the temperature profiles across a $1 \mu\text{m}$ thick diamond thin film. The results are plotted in terms of dimensionless temperature $T^+ = [T(z) - T_1] / [T_2 - T_1]$ and dimensionless time $\tau = \nu t / L$. Qualitatively, they compare well with results reported in the literature for $T_0 = 300$ K [12].

Figure 6 presents the steady-state temperature profiles across

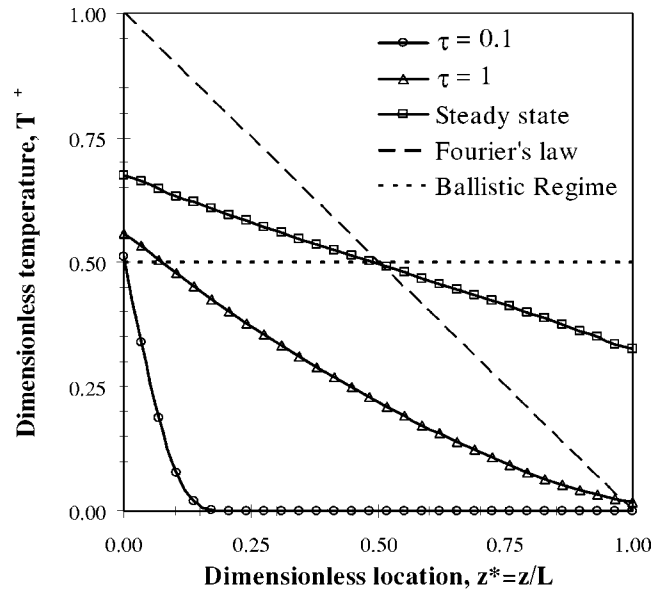


Fig. 5 Numerical solution for transient heat conduction across a $1 \mu\text{m}$ thick diamond type IIa thin film

diamond thin films having different thicknesses. One can see that the temperature gradient increases as the film thickness increases and that the numerical results fall between the acoustically thin (ballistic) and thick (Fourier's law) approximation limits. Similar results have been previously reported in the literature [3,11,12] for different temperatures and using other numerical schemes.

The present results confirm the good behavior of the numerical scheme for both transient and steady-state calculations, accounting for scattering on a spectral basis. Note that the actual time, and therefore the computational time, to reach steady-state increases with the film thickness.

4.3 Heat Conduction Along a Silicon Crystal Thin Film.

Phonon transport along a silicon crystal is considered in this section and schematically described in Fig. 7. The thin film is assumed to be a gray medium with a constant and uniform relax-

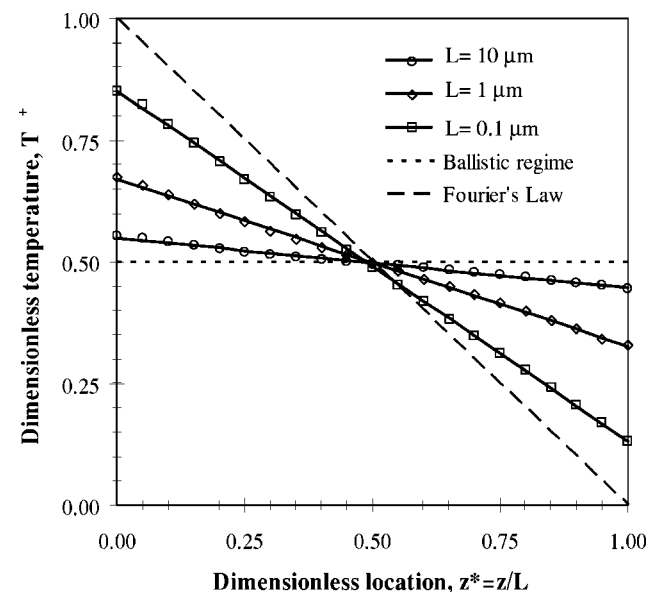


Fig. 6 Numerical solution for steady-state heat conduction across a diamond type IIa thin film of different thicknesses L

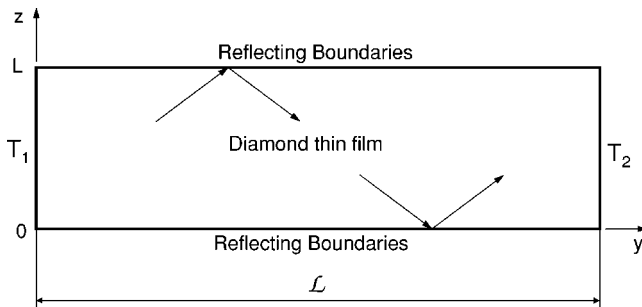
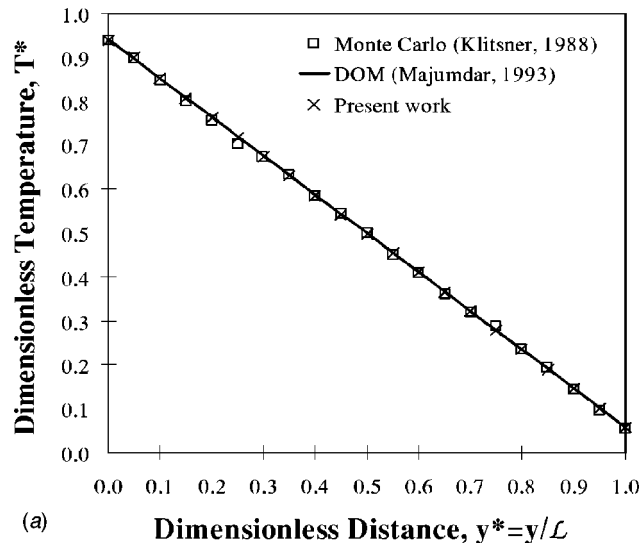


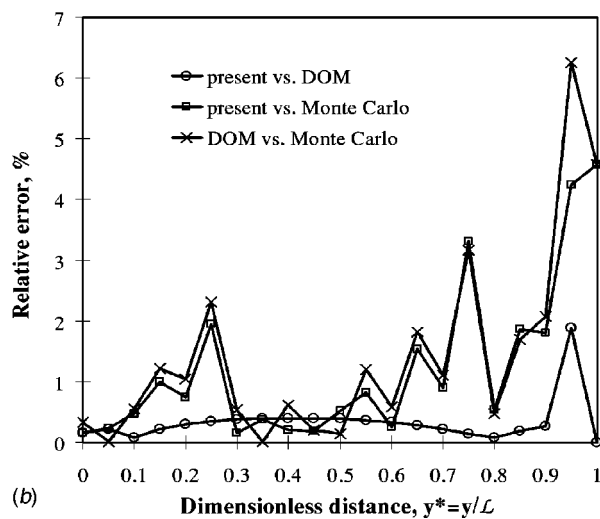
Fig. 7 Schematic for heat conduction problem along a silicon crystal thin film of length L

ation time defined as $\tau_s = \Lambda / \nu$, where Λ is the phonon mean free path that depends of the surface reflection [3,14] and the speed of sound in silicon ν is equal to 6400 m/s [29]. The lower ($z=0$) and upper ($z=L$) surfaces are specularly reflecting while the ends $y=0$ and $y=L$ are treated as black surfaces maintained at constant temperatures much below the silicon Debye temperature of 645 K.

Figure 8 compares the numerical results obtained by 1) the Monte Carlo method [14], 2) the discrete ordinate method [3,15],



(a)



(b)

Fig. 8 Comparison of numerical simulations of heat conduction along a $1 \mu\text{m}$ thick and $10 \mu\text{m}$ long silicon crystal thin-film.

and 3) the present method, for a silicon film with thickness $L=1 \mu\text{m}$ and length $\mathcal{L}=10 \mu\text{m}$. The results are given in dimensionless form with T^* given by Eq. (24) and $y^*=y/\mathcal{L}$. Figure 8 shows the relative difference between results obtained by the present method and those obtained by the Monte Carlo [14], and by the discrete ordinate methods [3] for specularly reflecting boundaries. The results compare very well with simulations reported in the literature [3,14]. The relative error between the present method and the DOM is less than 2%, while that with the Monte Carlo method is comparable to that between the DOM and the Monte Carlo method and stays below 6%. However, since no exact solution is available it is not possible to determine which method is the most accurate. Extension of the study to spectral diffuse surfaces and partially reflecting surfaces is straightforward. This test problem demonstrates the capability of the numerical scheme to deal with both 1D and 2D problems and with both black and specularly reflecting boundaries.

4.4 Discussion. The objective of the present paper is to demonstrate the capability of the modified method of characteristics to simulate microscale energy transport. Good agreement with reported results was shown. Similar or better stability and prediction capability than existing methods has been demonstrated. The numerical results have been obtained for 3D computational grids, and the program sequences, number of grid points, and directions have not been optimized. The scheme can be viewed as a hybrid method between the DOM and the ray tracing method. It is an alternative to that used by Coelho [30] for the radiative transfer equation. This section discusses trade-offs and compromises that can be made to achieve better numerical efficiencies.

First, the computational efficiency can be improved by approximating the integral present on the right-hand side of Eq. (17) by numerical quadrature. For example, given the symmetry of the above problems, the modified method of characteristics could have been used to solve the Schuster-Schwarzschild two-flux approximation by replacing the integral over all directions on the right-hand side of Eq. (7) by the sum of the positive and negative components [17]. In general, the computationally costly numerical integration over solid angle can be replaced by a weighted sum over an arbitrary number of discrete directions like in DOM. This procedure can significantly reduce the computational time, particularly for multidimensional and spectral calculations. It is recommended for optimization, real time transient calculations, and control of microscale devices. However, one will be faced with the same drawbacks inherent to the discrete ordinate method discussed in the Introduction. Similarly, the band approximation can be used for spectral calculations, as performed by Murthy and Mathur [11]. These approaches have not been retained here for the sake of accuracy, but they could easily be implemented for more complex problems or geometries.

Moreover, as discussed previously, the simulated boundary conditions were used in order to compare the results obtained by the present method with those reported in the literature. More realistic boundary conditions such as 1) diffusely reflecting opaque surfaces that are more appropriate for "acoustically rough" surfaces and 2) partially diffuse and specular reflecting boundaries as encountered in superlattices constitute an extension of the present work and can numerically be implemented with relative ease.

Finally, the present method is very well suited for parallel computing, since the intensity at each node at any time step depends explicitly and solely on the results obtained for the previous time step. The computing time can theoretically be divided by the number of grid points by using up to one CPU per grid point. Parallelization can significantly speed up the computation of the temperature field for real-time transient, multidimensional, and/or coupled problems, as well as for steady-state transport in optically thick media. In the diffusion approximation limit, when Fourier's law prevails, the governing equation becomes parabolic for transient and elliptic for steady-state heat conduction problems [25]. Parabolic equations feature repeated characteristics also having a

distinct domain of dependence and range of influence, but the signal propagates at infinite speed, unlike hyperbolic equations such as the BTE or the EPRT [25]. Elliptic equations have no real characteristics and their solutions at any grid point depend on the solution at all the other grid points. For both parabolic and elliptic equations, other numerical methods appear to be more appropriate than the present method [25].

5 Conclusions

This paper has described in detail a new numerical method for solving multidimensional transient and steady-state thermal transport at subcontinuum scale with black or reflecting boundaries on a gray or spectral basis. The modified method of characteristics is unconditionally stable, accurate, and compatible with other numerical schemes and can be used for coupled problems employing the same prespecified grid. The numerical solutions obtained for 1D and 2D heat conduction in dielectric thin films have been compared with the analytical solution and, when possible, with reported numerical results. Good agreement has been found confirming the capability of the numerical procedure and the associated computer program.

The numerical scheme developed in the present study could easily be extended to complex 3D geometry. The advantage of the proposed method is that even the most complicated problem can be solved with relative ease. As the problem becomes more realistic (in terms of geometry and coupling with electron or photon transport), the complexity of the formulation and the computational effort increase much more rapidly for conventional approaches. Furthermore, the method could also be used for 1) solving the RTE for emitting, absorbing, and scattering materials and 2) the BTE for electrons and holes as well as coupled electron-phonon-photon transport problems. It can be used for solving energy transport in subcontinuum regions in thermal or electrical contact with continuum regions where traditional methods can be used. The method is particularly recommended for transient, multidimensional, and/or coupled problems.

Acknowledgments

The author is indebted to Professor Raymond Viskanta and Professor Gang Chen, and to Dr. David Sung for their valuable comments and discussions. The author would like to acknowledge the comments of anonymous referees on the model assumptions and their physical meaning, as well as on the implementation and discussion of the boundary conditions.

Nomenclature

A	= constant
D_p	= density of states for polarization p , $m^{-3} s$
f	= heat carriers distribution function
h	= Planck's constant
\hbar	= Planck's constant divided by 2π , $1.054 \times 10^{-34} \text{ J s/photon}$
I_ω	= direction spectral phonon radiation intensity, $\text{J m}^{-2} \text{ sr}$
\vec{k}	= wavevector, m^{-1}
k_B	= Boltzmann constant, $1.38 \times 10^{-23} \text{ J/K phonon}$
L	= thin-film thickness, m
\mathcal{L}	= thin-film length (see Fig. 7)
n	= total number of heat carriers
\vec{p}	= particle momentum, kg m s^{-1}
\vec{q}	= heat flux vector, W m^{-2}
R	= radius of impurities
\vec{r}	= vector location
\vec{s}	= unit vector
t	= time, s
t^*	= dimensionless time, $t^* = vt/L$
T	= temperature, K

T^*	= dimensionless temperature,
$T^*(z)$	$= (T(z)^4 + T_2^4)/(T_1^4 + T_2^4)$
\vec{v}	= heat carrier group velocity vector, m/s
x	= longitudinal location, m
y	= spanwise location, m
z	= vertical location, m

Greek Symbols

Λ	= mean free path of the heat carriers, m
ν	= speed of sounds, m/s
ϵ	= energy of an individual heat carrier, J
μ	= director cosine, $\mu = \cos(\theta)$
ω	= phonon angular frequency, rad/s
ω_D	= Debye frequency, rad/s
ϕ	= azimuthal angle
η	= number of scatterings site per unit volume
φ	= scattering cross section of an impurity
θ_D	= Debye temperature, K
θ	= polar angle
σ	= Stefan-Boltzmann constant for phonons, $\text{W m}^{-2} \text{ K}^{-4}$
τ_i	= relaxation time for impurity scattering, s
τ_U	= relaxation time for Umklapp scattering, s
τ_s	= total relaxation time for scattering, s
τ^*	= acoustic thickness, $\tau^* = L/(\tau_s \nu)$

Subscripts

0	= refers to equilibrium
b	= refers to the boundary
e	= refers to electrons
i, j, k	= indices for the vector nodes of the computational grid
p	= polarization state

References

- Tien, C. L., and Chen, G., 1994, "Challenges in Microscale Conductive and Radiative Heat Transfer," *ASME J. Heat Transfer*, **116**, pp. 799–807.
- Tien, C. L., Majumdar, A., and Gerner, F. M. (eds.), 1997, *Microscale Energy Transport*, Taylor and Francis, London.
- Majumdar, A., 1993, "Microscale Heat Conduction in Dielectric Thin Films," *ASME J. Heat Transfer*, **115**, pp. 7–16.
- Kittel, C., 1996, *Introduction to Solid-state Physics*, Wiley, New York.
- Ramkrishna, D., 2000, *Population Balances*, Academic Press, San Diego.
- Goodson, K. E., Ju, Y. S., and Asheghi, M., 1997, "Thermal Phenomena in Semiconductor Devices and Interconnects," *Microscale Energy Transport*, Taylor and Francis, London, pp. 229–288.
- Majumdar, A., 1997, "Microscale Energy Transport in Solids," in *Microscale Energy Transport*, Taylor and Francis, pp. 3–93.
- Kumar, S., and Ramkrishna, D., 1996, "On the Solution of Population Balance Equation by Discretization—I a Fixed Pivot Technique," *Chem. Eng. Sci.*, **51**(8), pp. 1311–1332.
- Kumar, S., and Ramkrishna, D., 1997, "On the Solution of Population Balance Equation by Discretization—III Nucleation, Growth, and Aggregation of Particles," *Chem. Eng. Sci.*, **52**(4), pp. 4659–4679.
- Chen, G., 2001, "Ballistic-Diffusive Heat-Conduction Equations," *Phys. Rev. Lett.*, **86**(11), pp. 2297–2300.
- Murthy, J., and Mathur, S. R., 2002, "Computation of Sub-Micron Thermal Transport Using an Unstructured Finite Volume Method," *ASME J. Heat Transfer*, **124**, pp. 1176–1181.
- Joshi, A. A., and Majumdar, A., 1993, "Transient Ballistic and Diffusive Phonon Heat Transport in Thin Films," *J. Appl. Phys.*, **74**(1), pp. 31–39.
- Sverdrup, P. G., Ju, Y. S., and Goodson, K. E., 2001, "Sub-Continuum Simulations of Heat Conduction in Silicon-on-Insulator Transistors," *ASME J. Heat Transfer*, **123**, pp. 130–137.
- Klitsner, T., VanCleve, J. E., Fisher, H. E., and Pohl, R. O., 1988, "Phonon Radiative Heat Transfer and Surface Scattering," *Phys. Rev. B*, **38**(11), pp. 7576–7594.
- Kumar, S., Majumdar, A., and Tien, C. L., 1990, "The Differential-Discrete-Ordinate Method for Solving the General Equation of Radiative Transfer," *ASME J. Heat Transfer*, **112**, pp. 424–429.
- Chai, J. C., Lee, H. S., and Patankar, S. V., 1993, "Ray Effect and False Scattering in the Discrete Ordinates Method," *Numer. Heat Transfer, Part B*, **24**, pp. 373–389.
- Modest, M. F., 1993, *Radiative Heat Transfer*, McGraw-Hill, New York, NY.
- Murthy, J., and Mathur, S. R., 2003, "An Improved Computational Procedure for Sub-Micron Heat Conduction," *ASME J. Heat Transfer*, **125**, pp. 904–910.
- Truelove, J. S., 1987, "Discrete-Ordinate Solutions of the Radiative Transport Equation," *ASME J. Heat Transfer*, **109**, pp. 1048–1051.
- Raithby, G. D., 1994, "Discussion of the Finite-Volume Method for Radiation

- and its Application Using 3D Unstructured Meshes,” *Numer. Heat Transfer, Part B*, **35**, pp. 389–405.
- [21] Modest, M. F., 2003, “Backward Monte Carlo Simulations in Radiative Heat Transfer,” *ASME J. Heat Transfer*, **125**, pp. 57–62.
- [22] Pilon, L., and Viskanta, R., 2003, “Modified Method of Characteristics for Solving the Population Balance Equation,” *Int. J. Numer. Methods Fluids*, **42**, pp. 1211–1236.
- [23] Zeng, T., and Chen, G., 2001, “Phonon Heat Conduction in Thin Films: Impact of Thermal Boundary Resistance and Internal Heat Generation,” *ASME J. Heat Transfer*, **123**, pp. 340–347.
- [24] Allievi, A., and Bermejo, R., 2000, “Finite Element Modified Method of Characteristics for Navier-Stokes Equations,” *Int. J. Numer. Methods Fluids*, **32**, pp. 439–464.
- [25] Hoffman, J. D., 1998, *Numerical Methods for Engineers and Scientists*, McGraw-Hill, New York.
- [26] Marcum, D. L., 1985, *Calculation of three-dimensional inviscid flowfields*, PhD thesis, Purdue University.
- [27] Patankar, S., 1980, *Numerical Heat Transfer and Fluid Flow*, Hemisphere, Washington, DC.
- [28] Mazumder, S., and Majumdar, A., 2001, “Monte Carlo Study of Phonon Transport in Solid Thin Films Including Dispersion and Polarization,” *ASME J. Heat Transfer*, **123**, pp. 749–759.
- [29] Holland, M. G., 1964, “Analysis of Lattice Thermal Conductivity,” *Phys. Rev.*, **134**(2A), pp. A471–480.
- [30] Coelho, P. J., 2002, “Bounded skew high-order resolution schemes for the discrete ordinates method,” *J. Computational Physics*, **175**(2) pp. 412–437.